

## Mathematical Modeling and Characterization of Thin Film, Narrow Gap Sensor Array Units (SAU)

Mahmoud Z. Iskandarani  
Department of Electrical Engineering, Faculty of Engineering,  
Al-Zaytoonah Private University of Jordan,  
P.O. Box 911597, Post Code 11191, Amman, Jordan

---

**Abstract:** Design, modeling, testing and analysis multi-gap PbPc sensor array units for the purpose of gas detection are carried out. The tested devices showed reduction in conductance as a function of increasing gap width and reducing film thickness and an increase as a function of temperature up to 160°C. An observed morphological change in the sublimed film is realized at 190°C as the conductance of the sensor array started to drop. Analytical modeling using semi-infinite coplanar electrode arrangement supported the obtained testing results. **Problem statement:** Stability in gas detection and subsequent discrimination is closely related to sensor design and test parameter and its response to an applied set of chemicals. **Approach:** To enhance sensor performance and improve sensor designs, a suggested design with mathematical analysis and gas response analysis is carried out. **Results:** A solid analytical mathematical model is established with both electric field and conductance equations. Effect of deposited sensor film thickness and inter-electrode separation on its response is also established and proved through practical test data. **Conclusion:** The obtained experimental results agree with the derived mathematical solutions.

**Key words:** Electronic nose, mathematical modeling, phthalocyanine, thin film, conductivity, sensor arrays, biometrics, sensor array units

---

### INTRODUCTION

The observation that the semi conducting properties of phthalocyanines are modulated by the adsorption and desorption of gases led to their incorporation as chemical sensors. In addition, the ability to manipulate them as micro electronic device compatible thin films with good chemical and thermal stability and gas specificity by choice of metal substitutes made them favorable for sensing applications (Jakubik *et al.*, 2008; Paoletti *et al.*, 2009; Li *et al.*, 2008; Liu *et al.*, 2004; Shi and Ramprasad, 2007).

With the advancement of microelectronic technology, it becomes possible to produce Metal-Phthalocyanine sensors that can be operated at low potential levels. Metal-Phthalocyanine (MPc) based sensor forms a weak bond with gases and suffers a noticeable change in its conductivity, which is believed to be a result of a donor-acceptor complex formation. Accepting gases can cause a large increase in the sensor conductivity with a decrease in its activation energy and occurrence of charge transfer bonds. On the other hand, donor gases have an opposite effect on the deposited sensing films. Hence, Phthalocyanine sensors are p-type semi conducting materials.

Nitrogen Dioxide has a large effect (up to 8 orders of magnitude) on the surface conductivity of a variety of sublimed Phthalocyanine films accompanied by large changes in activation energies.

Experimental study showed that Lead Phthalocyanine (PbPc) is the most sensitive complex to Dioxide gases; in particular NO<sub>2</sub>, as its conductivity affected more by the adsorption of testing gases as a charge-transfer complex is formed between the Phthalocyanine donor and the gas acceptor.

Phthalocyanine is a large planar molecule with an extensive delocalized  $\pi$ -electron system. Also, most of its metal complexes are also planar. However, with metals such as Lead (Pb) which are too large to fit into the space between the four central Nitrogen atoms, PbPc molecules show significant non-planarity. In the solid state the intermolecular forces between these large molecules are predominantly attractive dispersion forces, which are not strongly directional in nature and short range repulsion forces. As in many molecular crystals, this leads to polymorphism, where several different molecular packing arrangements being possible with similar overall lattice energy. The planar metal phthalocyanines have two common polymorphic forms,  $\alpha$  and  $\beta$ , whose structures are both monoclinic.

The non-planar lead Phthalocyanine (PbPc) also has two principle polymorphs:

- The triclinic form obtained by entrainer sublimation growth with the cool zone at 320°C with four molecules per unit, all arranged in two crystal graphically independent but almost identical molecular stacks. Each stack consists of alternate convex and concave non-planar molecules inclined at about 60° to the stacking axis
- The monoclinic form obtained in a similar manner but with cool zone at 250°C with stacks of molecules arranged like a pile of saucers, with all the molecules within each stack out-of-plane in the same sense and the lead atoms directly above each other

The extensive structural information is of considerable significance for the interpretation of transport and optical properties. Charge transport in crystalline phthalocyanines may be regarded as occurring by either.

**Narrow band mechanism:** Charge carrier mobility is directly related to the intermolecular overlap integral, or, by intermolecular hopping process where, the energy barrier to be traversal in each individual jump between two molecules depends on relative orientations and separations of adjacent molecules and hence on the crystal structure (Park *et al.*, 2009; Brunet *et al.*, 2008; Craciun *et al.*, 2006; Tans *et al.*, 2003; Bohrer *et al.*, 2009).

Sensing systems have an excellent capabilities extracting very specific information from an array of inputs. It is assumed that such sensory processing capability would consist of highly precise sensors as the fundamental building blocks of the processing systems. However, it is not the case. Sensing and discrimination in practical systems rely on large arrays to provide redundancy, overcome low precision in individual sensors with good interconnectivity to provide comprehensive data coupled with diverse topology. Some standalone chemical sensors suffer many problems with reproducibility, selectivity, sensitivity, stability and response time (Mamishhev *et al.*, 2004; Chen *et al.*, 2004; Hong *et al.*, 2005; Schmied, 2010).

The individual chemical sensor is successful in detecting particular chemicals. However, in sensing environments that are potentially visited by chemical mixtures, false readings can often occur. Such discrimination errors, leading to poor selectivity are associated with many chemical sensors. Most sensors are inherently sensitive to a wide variety of chemicals. Part of the solution is the implementation of arrays of chemical

sensors; designed properly with appropriate signal processing techniques (Shen *et al.*, 2009; Chen *et al.*, 2009; Mahdi *et al.*, 2010; Abdullah *et al.*, 2010; Radhi *et al.*, 2010; Abdalrazaq *et al.*, 2010).

In this study tested multi-gap chemical sensor array units will be mathematically modeled and their practical results analyzed.

## MATERIALS AND METHODS

A number of SAU having different gap widths with vacuum sublimed PbPc films of different thicknesses on sapphire ( $\alpha\text{-Al}_2\text{O}_3$ ) substrates are produced as shown in Fig. 1.

Testing of the devices response to donor gases in particular  $\text{NO}_2$  is carried out under computer control in a specifically designed temperature controlled stainless steel testing cells. Each testing cell formed an array of three multi-gap (three gaps) chemiresistors making an overall array of nine sensing elements per testing cell. Experimental setup is shown in Fig. 2.



Fig. 1: PbPc Sensor Array Unit (SAU)

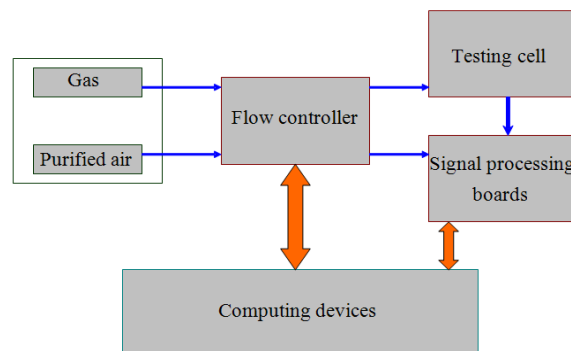


Fig. 2: SAU array testing system

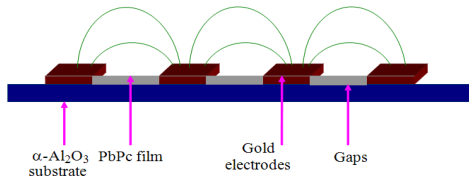


Fig. 3: SAU cross section

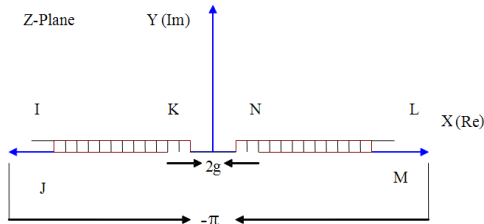


Fig. 4: Coplanar electrodes cross section

A cross-section of the sensor array unit structure is modeled as shown in Fig. 3. As the each electrode length is much larger than the separating gap with very thin pbpc sublimed film, each sau is modeled as a semi-infinite coplanar electrode device integrated on the sapphire substrate (Rettig and Moos, 2009; Huang and Wan, 2009; Zeng *et al.*, 2009; Sugiyasu and Swager, 2007; Lange *et al.*, 2009).

Each two co-planar electrodes in the z-plane correspond to two divergent sides of a polygon extending at infinity with a negative vertex angle and six vertices i, j, k and l, m, n (Fig. 4). But since i, j and l, m reach infinity with an angle of  $-\pi$  and k and n are symmetrical about the y-axis, then the polygonal boundary can be considered to form a three vertices polygon, namely l, m and n; with k and n having interior angles of  $2\pi$  with respects to the x-axis as shown in Fig. 5. A conformal transformation of the real axis of the t-plane, (Fig. 6), into the interior of the polygon, (Fig. 5) is carried out.

Let the vertex m in the z-plane correspond with the limit as and assume the following correspondence between the remaining points and vertices:

- at n,  $t = +1, z = +g, \theta_1 = 2\pi$
- at -n,  $t = -1, z = -g, \theta_2 = 2\pi$
- at l,  $t = 0, z = \infty, \theta_3 = -\pi$

Substitution of these points in the schwarz-christoffel differential equation given by:

$$\frac{dz}{dt} = C_1(t-t_1)\left(\frac{\theta_1}{\pi}\right)^{-1} (t-t_2)\left(\frac{\theta_2}{\pi}\right)^{-1} \dots(t-t_n)\left(\frac{\theta_n}{\pi}\right)^{-1} \quad (1)$$

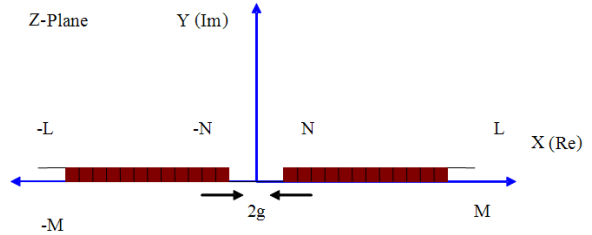


Fig. 5: Z-plane geometrical mapping

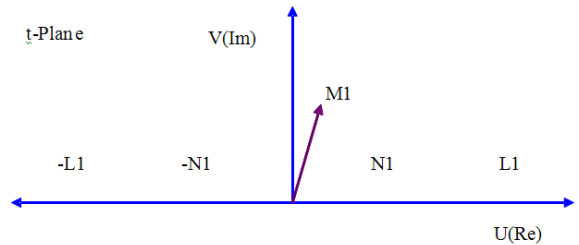


Fig. 6: t-plane mathematical mapping

Yields:

$$\frac{dz}{dt} = C_1(t^2 - 1)(t^{-2}) = C_1(1 - t^{-2}) \quad (2)$$

Integrating (2) gives:

$$z = f_1(t) = \int dz = C_1 \int (1 - t^{-2}) dt = C_1 \left( t + \frac{1}{t} \right) + K_1 \quad (3)$$

where, constants  $C_1$  and  $K_1$  depend on the correspondence between the points in the two planes. Applying boundary conditions (a) and (b):

$$d = 2C_1 + K_1 - d = -2C_1 + K_1 \quad (4)$$

Solving for  $C_1$  and  $K_1$  gives:

$$C_1 = \frac{d}{2} K_1 = 0 \quad (5)$$

The transformation expression can now be obtained by substituting (5) into (3) as:

$$z = \frac{d}{2} \left( t + \frac{1}{t} \right) \quad (6)$$

The expression in Eq. 6 has a pole at  $t = 0$ , which corresponds to the infinite side of the co-planar electrodes and satisfies boundary condition (c) for  $z = \infty$  at  $t = 0$ .

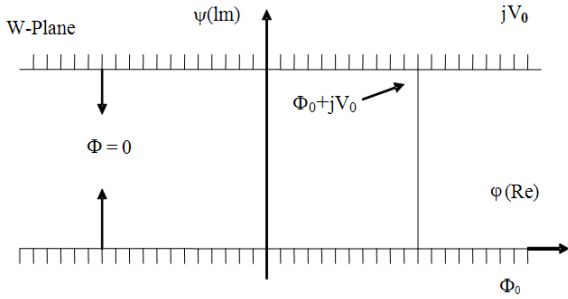


Fig. 7: Electrical transformation into W-plane

To the required Electrical Transformation, the coplanar electrode on the positive x-axis in the z-plane is rotated by an angle  $\pi$  (anti clockwise) so the two semi-infinite coplanar electrodes will be transformed to two infinite parallel lines which are used in the W-plane to form a polygon as shown in Fig. 7.

When rotated, vertices will meet at infinity with a vertex angle of zero and the boundary conditions become as follows:

- (a) At  $w = \infty + jV_0, t = -\infty$
- (b) At  $w = \infty, t = \infty$
- (c) At  $w = -\infty, t = 0, \phi = 0$

These boundary conditions describe a polygon with a single vertex. Now applying the following equation:

$$\frac{dw}{dt} = C_2(t-t_1)\left(\frac{\theta_1}{\pi}\right)^{-1} (t-t_2)\left(\frac{\theta_2}{\pi}\right)^{-1} \dots (t-t_n)\left(\frac{\theta_n}{\pi}\right)^{-1} \quad (7)$$

Gives:

$$\frac{dw}{dt} = C_2 t^{-1} \quad (8)$$

Integration of Eq. 8 gives:

$$w = f_2(t) = \int dw = C_2 \int t^{-1} dt = C_2 \ln(t) + K_2 \quad (9)$$

Since points  $w = -\infty$  and  $t = 0$  are made to correspond, then  $K_2 = 0$  and (9) reduces to:

$$w = C_2 \ln(t) \quad (10)$$

As the semi-infinite coplanar electrode on the positive x-axis is rotated by an angle  $\pi$  to produce the two parallel lines in the w-plane; a semi-circular arc is formed in the t-plane with radius R with the following points corresponding to each other:

$$w = \phi_0 \Rightarrow \text{Re} \exp(j0) = R$$

$$w = \phi_0 + jV_0 \Rightarrow t = \text{Re} \exp(j\pi)$$

Substituting these points in equation (10) yields:

$$\phi_0 = C_2 \ln(R) \quad (11)$$

$$\phi_0 + jV_0 = C_2(\ln(R) + j\pi)$$

Solving for  $C_2$  gives:

$$C_2 = \frac{V_0}{\pi} \quad (12)$$

Substituting (12) into (10) gives the equation of the electrical transformation as:

$$C_2 = \frac{V_0}{\pi} \ln(t) \quad (13)$$

Equation 13 is only defined for  $t > 0$  and it has a zero at  $t = 1$  and satisfies the boundary condition (c) at  $t = 0$ . To obtain the complete conformal transformation, the variable t needs to be eliminated as follows:

$$t = \exp\left(\frac{\pi w}{V_0}\right) \quad (14)$$

Substituting (14) into (6) gives:

$$z = g \left[ \frac{\exp\left(\frac{\pi w}{V_0}\right) + \exp\left(-\frac{\pi w}{V_0}\right)}{2} \right] = g \cosh\left(\frac{\pi w}{V_0}\right) \quad (15)$$

Hence, the complete transformation expression becomes:

$$w = \frac{V_0}{\pi} \cosh^{-1}\left(\frac{z}{g}\right) \quad (16)$$

The field strength expression is given as the gradient of the potential, so:

$$|\underline{E}| = E = \left| \frac{dw}{dz} \right| = \left| \frac{d}{dz} \left( \frac{V_0}{\pi} \cosh^{-1}\left(\frac{z}{g}\right) \right) \right| = \left| \frac{V_0}{\pi(z^2 - g^2)^{1/2}} \right| \quad (17)$$

Two cases need to be discussed to establish gap width and film thickness effect on device conductivity:

(I)  $x = 0$ : The relationship between film thickness and gap width is established as the dominant field is in the  $y$ -direction along the sublimed film height. Equation 17 becomes:

$$E_y = \left| \frac{V_0}{\pi(-y^2 - g^2)^{1/2}} \right| = \left| \frac{V_0}{j\pi(y^2 + g^2)^{1/2}} \right| = \frac{V_0}{\pi(y^2 + g^2)^{1/2}} \quad (18)$$

Integrating (18) gives:

$$V_y = \frac{V_0}{\pi} \sinh^{-1} \left( \frac{y}{g} \right) = \frac{V_0}{\pi} \ln \left[ \left( \frac{y}{g} \right) + \sqrt{\left( \left( \frac{y}{g} \right)^2 + 1 \right)} \right] \quad (19)$$

The device conductance under these conditions is given by:

$$G_{y(\text{SteadyState})} = \frac{G_0}{\pi} \ln \left[ \left( \frac{y}{g} \right) + \sqrt{\left( \left( \frac{y}{g} \right)^2 + 1 \right)} \right] \quad (20)$$

(II)  $y = 0$ : The relationship between gap width and travelled distance (electrode length) is established as the dominant field is in the  $x$ -direction along the sublimed film length. Equation 17 becomes:

$$E = \left| \frac{V_0}{\pi(x^2 - g^2)^{1/2}} \right| \quad (21)$$

Integrating (21) gives:

$$V_x = \frac{V_0}{\pi} \cosh^{-1} \left( \frac{x}{g} \right) = \frac{V_0}{\pi} \ln \left[ \left( \frac{x}{g} \right) + \sqrt{\left( \left( \frac{x}{g} \right)^2 - 1 \right)} \right] \quad (22)$$

Equation 22 is valid for  $x > g$ .

The device conductance under these conditions is given by:

$$G_{x(\text{SteadyState})} = \frac{G_0}{\pi} \ln \left[ \left( \frac{x}{g} \right) + \sqrt{\left( \left( \frac{x}{g} \right)^2 - 1 \right)} \right] \quad (23)$$

## RESULTS

Table 1-3 present the obtained practical measurements for 9 SAU devices.

Figure 8-9 show effect of gap width on SAU conductance for a series of incrementally applied  $\text{NO}_2$  gas concentrations. From the plots, it is realized the inverse relationship between device conductance and

gap width with a shape function consistent with the derived analytical functions in Eq. 23. Figure 10-12 show temperature effect on the conductance of each gap, where morphological change is obvious at  $190^\circ\text{C}$ . Such change is noticed to have least effect on the largest gap, which is due to the overall, sublimed film surface area being larger. Figure 13 shows effect of sublimed film thickness on the level of conductance as a response of series of subjecting the SAU device to a series of  $\text{NO}_2$  concentrations. The plot shows an increase in device conductance as a function of film thickness with some non-linearity at 1500 nm due to bulk activities. This result is in agreement with Eq. 20.

Table1: Variable thickness SAU with fixed 10  $\mu\text{M}$  GAPS

$C_0$ (PPM)	$G \times 10^{-7}$ (500 nm)	$G \times 10^{-7}$ (y = 1000 nm)	$G \times 10^{-7}$ (y = 1500 nm)
<b>Temperature = 130</b>			
0	0.0000	0.0000	0.0000
1	0.3922	0.8911	1.9448
3	0.8851	1.6941	2.4200
5	1.2170	2.1203	2.9530
7	1.4810	2.4135	3.2980
9	1.6750	2.6320	3.6040
<b>Temperature = 160</b>			
0	0.0000	0	0.0000
1	0.7727	1.3956	1.9694
3	1.2743	2.0646	2.6754
5	1.6214	2.4752	3.2515
7	1.8952	2.7772	3.6996
9	2.1042	3.0139	4.0463
<b>Temperature = 190</b>			
0	0.0000	0.0000	0.0000
1	0.4020	1.4014	1.9324
3	0.7332	1.7226	2.3533
5	0.9837	2.0640	2.7130
7	1.1901	2.3722	3.0675
9	1.3360	2.5754	3.3071

Table 2: Variable gap width SAU with fixed 1000 nm films

$C_0$ PPM	$G \times 10^{-7}$ (10 $\mu\text{m}$ )	$G \times 10^{-7}$ (33 $\mu\text{m}$ )	$G \times 10^{-7}$ (100 $\mu\text{m}$ )
<b>Temperature = 130</b>			
0	0.0000	0.0000	0.0000
1	0.4886	0.3179	0.1761
3	0.9248	0.6251	0.4165
5	1.1995	0.8278	0.5722
7	1.3560	0.9528	0.6743
9	1.4871	1.0520	0.7513
<b>Temperature = 160</b>			
0	0.0000	0.0000	0.0000
1	0.6391	0.4271	0.2224
3	1.1613	0.8085	0.5091
5	1.3932	1.0090	0.6641
7	1.5446	1.1133	0.7462
9	1.6026	1.1747	0.7941
<b>Temperature = 190</b>			
0	0.0000	0.0000	0.0000
1	0.6438	0.4264	0.1905
3	0.8272	0.5512	0.2910
5	0.9697	0.6590	0.3718
7	1.0882	0.7469	0.4375
9	1.1710	0.8152	0.4864

Table 3: Variable gap width SAU with fixed 1000 nm films

C <sub>0</sub> PPM	G×10 <sup>-7</sup> (5 μm)	G×10 <sup>-7</sup> (10 μm)	G×10 <sup>-7</sup> (15μm)
<b>Temperature 130</b>			
0	0.0000	0.0000	0.0000
1	0.9836	0.7675	0.5793
3	1.5305	1.2846	0.9866
5	1.9030	1.6617	1.2930
7	2.1414	1.9203	1.4924
9	2.2944	2.1037	1.6488
<b>Temperature = 160</b>			
0	0.0000	0.0000	0.0000
1	1.2448	1.0004	0.7646
3	1.8745	1.6158	1.2645
5	2.2602	2.0678	1.6163
7	2.5210	2.3294	1.8364
9	2.6441	2.5068	1.9902
<b>Temperature = 190</b>			
0	0.0000	0.0000	0.0000
1	1.3603	1.1321	0.9107
3	1.6835	1.4482	1.1725
5	1.9661	1.7054	1.3863
7	2.1486	1.9117	1.5522
9	2.3020	2.0891	1.6849

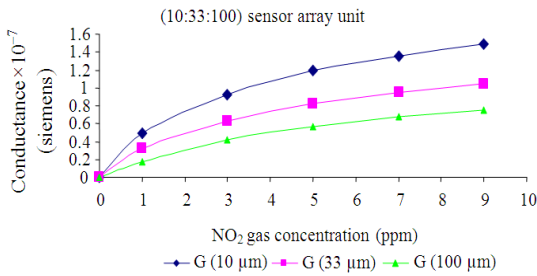


Fig. 8: Effect of gap width on SAU conductance

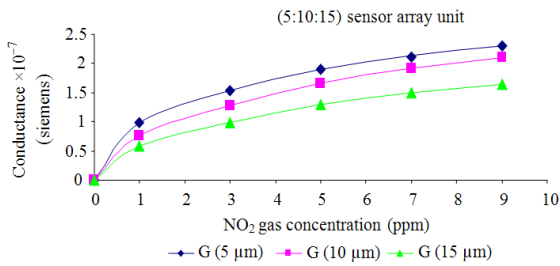


Fig. 9: Effect of gap width on SAU conductance

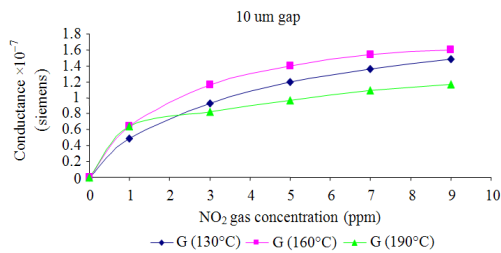


Fig. 10: Temperature effect on SAU conductance

Figure 14-16 show temperature effect on each film thickness for fixed gap widths with highest thickness showing larger effect due to bulk activities.

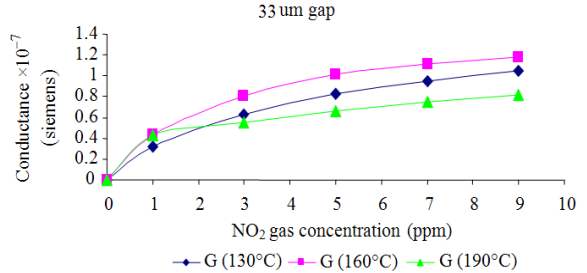


Fig. 11: Temperature effect on SAU conductance

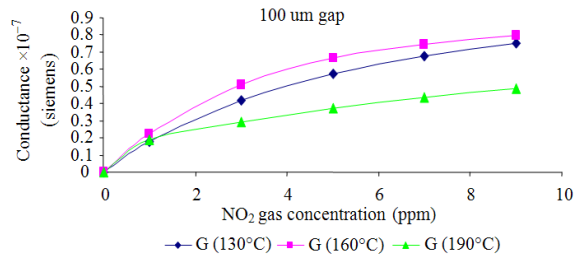


Fig. 12: Temperature effect on SAU conductance

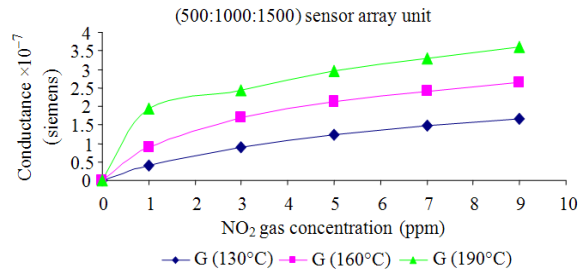


Fig. 13: Effect of film thickness on SAU conductance

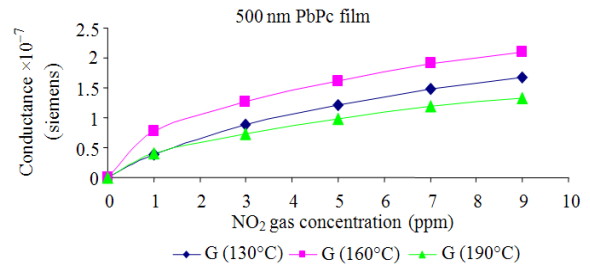


Fig. 14: Temperature Effect on SAU conductance

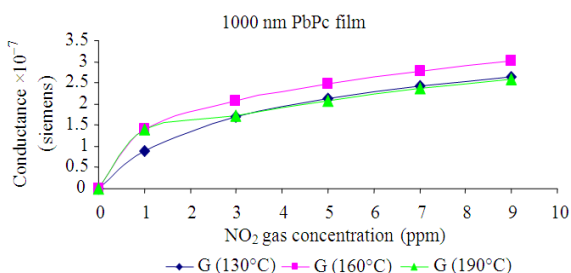


Fig. 15: Temperature effect on SAU conductance

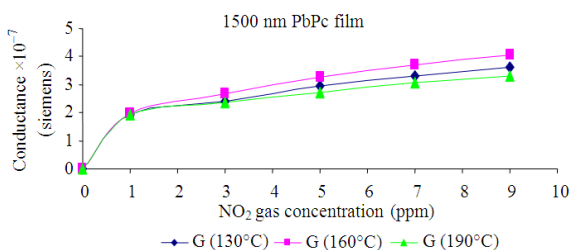


Fig. 16: Temperature effect on SAU conductance

### DISCUSSION

Analytical solution and the available practical measurements show a reduction in the conductance of a multi-gap sensors array as a function of:

- Gap Width increase
- Film Thickness decrease
- Temperature increase above 160°C

The provided data and solution indicate an increase in the conductance as a function of:

- Temperature increase up to 160°C
- Gas Concentration increase

Such observations are related to the adsorption-desorption of the NO<sub>2</sub> gas, which is determined by the energy of the NO<sub>2</sub> species and the activation energy required for the gas molecules to be adsorbed. If there are still some molecules covering the sublimed film surface at the application of an NO<sub>2</sub> concentration, then the larger the gap, the more expected molecules to exist with repulsion between them and new applied species and multi-layer physisorption also engaged in process. As the sublimed film thickness increases, more active sites are available to be populated by PbPc molecules, increasing the overall conductance per temperature and phase. Such increase in sensors conductance is even

higher at higher temperatures due to the chemisorption mechanism being the dominant mechanism. This is true up to the point (T = 190°C) where morphological changes are induced, removing most of the surface adsorption sites as surface reconstruction occurs. However, effect of increasing gas concentration at different morphological structures is shown to increase conductance of the sensors as the gas pressure increases over the film surface.

### CONCLUSION

The PbPC SAU proved to be sensitive to NO<sub>2</sub> Gas with the following parameters controlling the devices response:

- Gap Width
- Film Thickness
- Temperature

### REFERENCES

- Abdalrazaq, E.A., O.M. Al-Ramadane and K.S. Al-Numa, 2010. Synthesis and characterization of dinuclear metal complexes stabilized by tetradentate schiff base ligands. *Am. J. Applied Sci.*, 7: 628-633. <http://www.scipub.org/fulltext/ajas/ajas75628-633.pdf>
- Abdullah, W.F.H., M. Othman, M.A.M. Ali and M.S. Islam, 2010. Knowledge representation of ion-sensitive field-effect transistor voltage response for potassium ion concentration detection in mixed potassium/ammonium ion solutions. *Am. J. Applied Sci.*, 7: 81-88. <http://www.scipub.org/fulltext/ajas/ajas7181-88.pdf>
- Bohrer, F.I., C.N. Colesniuc, J. Park, M.E. Ruidiaz and I.K. Schuller *et al.*, 2009. Comparative gas sensing in cobalt, nickel, copper, zinc and metal-free phthalocyanine chemiresistors. *J. Am. Chem. Soc.*, 131: 478-485. DOI: 10.1021/ja803531r
- Brunet, J., A. Pauly, C. Varenne, B. Lauron, 2008. On-board phthalocyanine gas sensor microsystem dedicated to the monitoring of oxidizing gases level in passenger compartments. *Sensors Actuat. B: Chem.*, 130: 908-916. DOI: 10.1016/j.snb.2007.10.074
- Chen, J.Z., A.A. Darhuber, S.M. Troian and S. Wagner, 2004. Capacitive sensing of droplets for microfluidic devices based on thermocapillary actuation. *Lab Chip*, 4: 473-480. DOI: 10.1039/b315815b

- Chen, P.C., F.N. Ishikawa, H.K. Chang, K. Ryu and C. Zhou, 2009. A nanoelectronic nose: A hybrid anowire/carbon nanotube sensor array with integrated micromachined hotplates or sensitive gas discrimination. *Nanotechnology*, 20: 1-8. DOI: 10.1088/0957-4484/20/12/125503
- Craciun, M.F., S.R. Rogge, M.J.L. den Boer, S. Margadonna and K. Prassides *et al.*, 2006. Electronic transport through electron-doped metal phthalocyanine materials. *Adv. Mater.*, 18: 320-324. DOI: 10.1002/adma.200501268
- Hong, J., D.S. Yoon, S.K. Kim, T.S. Kim and S. Kim *et al.*, 2005. AC frequency characteristics of coplanar impedance sensors as design parameters. *Lab. Chip*, 5: 270-279. DOI: 10.1039/b410325d
- Huang, J. and Q. Wan, 2009. Gas sensors based on semiconducting metal oxide one-dimensional nanostructures. *Sensors*, 9: 9903-9924. DOI: 10.3390/s91209903
- Jakubik, W.P., M. Urbanczyk, E. Maciak and T. Pustelny, 2008. Surface acoustic wave hydrogen gas sensor based on layered structure of palladium/metal-free phthalocyanine. *Bull. Polish Acad. Sci. Tech. Sci.*, 56: 133-138. [http://www.ippt.gov.pl/~bulletin/\(56-2\)133.pdf](http://www.ippt.gov.pl/~bulletin/(56-2)133.pdf)
- Lange, U., N.V. Roznyatovskaya and V.M. Mirsky, 2009. Conducting polymers in chemical sensors and arrays. *Anal. Chim. Acta*, 614: 1-26. DOI: 10.1016/j.aca.2008.02.068
- Li, L., Q. Tang, H. Li, W. Hu and X. Yang *et al.*, 2008. Organic thin-film transistors of phthalocyanines. *Pure Applied Chem.*, 80: 2231-2240. DOI: 10.1351/pac200880112231
- Liu, Z., H. Kwok, A.B. Djuricic, 2004. The optical functions of metal phthalocyanines. *J. Phys. D: Applied Phys.*, 37: 678-688. DOI: 10.1088/0022-3727/37/5/006
- Mahdi, H.J., R. Andayani and Ishak, 2010. Metabolic fingerprinting of three malaysian ginger (*Zingiber officinale* Roscoe) using gas chromatography-mass spectrometry. *Am. J. Applied Sci.*, 7: 17-23. <http://www.scipub.org/fulltext/ajas/ajas7117-23.pdf>
- Mamishhev, A.V., K. Sundara-Rajan, F. Yang, Y. Du and M. Zahn, 2004. Interdigital sensors and transducers. *Proc. IEEE*, 92: 808-845. DOI: 10.1109/JPROC.2004.826603
- Paoletti, A.M., G. Pennesi, G. Rossi, A. Generosi and B. Paci *et al.*, 2009. Titanium and ruthenium phthalocyanines for NO<sub>2</sub> sensors: A mini-review. *Sensors*, 9: 5277-5297. DOI: 10.3390/s90705277
- Park, J., J.E. Royer, C.N. Colesniuc, F.I. Bohrer and A. Sharoni *et al.*, 2009. Ambient induced degradation and chemically activated recovery in copper phthalocyanine thin film transistors. *J. Applied Phys.*, 106: 1-8. DOI: 10.1063/1.3159885
- Radhi, M.M., W.T. Tan, M.Z.B.A. Rahman and A.B. Kassim, 2010. Voltammetric detection of Mn(II) in blood sample at C<sub>60</sub> and MWCNT modified glassy carbon electrodes. *Am. J. Applied Sci.*, 7: 395-401. <http://www.scipub.org/fulltext/ajas/ajas73395-401.pdf>
- Rettig, F. and R. Moos, 2009. Temperature-modulated direct thermoelectric gas sensors: Thermal modeling and results for fast hydrocarbon sensors. *Meas. Sci. Technol.*, 20: 1-9. DOI: 10.1088/0957-0233/20/6/065205
- Schmied, R., 2010. Electrostatics of gapped and finite surface electrodes. *New J. Phys.*, 12: 1-16. DOI: 10.1088/1367-2630/12/2/023038
- Shen, G., P.C. Chen, K. Ryu and C. Zhou, 2009. Devices and chemical sensing applications of metal oxide nanowires. *J. Mater. Chem.*, 19: 828-839. DOI: 10.1039/b816543b
- Shi, N. and R. Ramprasad, 2007. Intrinsic dielectric properties of phthalocyanine crystals: An *ab initio* investigation. *Phys. Rev., B* 75: 1-7. DOI: 10.1103/PhysRevB.75.155429
- Sugiyasu, K. and T.M. Swager, 2007. Conducting-polymer-based chemical sensors: Transduction mechanisms. *Bull. Chem. Soc. Jap.*, 80: 2074-2083. DOI: 10.1246/bcsj.80.2074
- Tans, S.J., R.G. Miedema, L.J. Geerligs, C. Dekker and J. Wu *et al.*, 2003. Electronic transport in monolayers of phthalocyanine polymers. *Nanotechnology*, 14: 1043-1050. DOI: 10.1088/0957-4484/14/9/320
- Zeng, W., T. Liu, Z. Wang, S. Tsukimoto and M. Saito *et al.*, 2009. Selective detection of formaldehyde gas using a Cd-Doped TiO<sub>2</sub>-SnO<sub>2</sub> sensor. *Sensors*, 9: 9029-9038. DOI: 10.3390/s91109029